Comparison of p-type a-Si:C:H/ZnO:Al and μc-Si:C:H/ZnO:Al Thin-film Solar Cell Structures – A Hard X-ray Photoelectron Spectroscopy Study

D. Gerlach,[1] D. Wippler,[2] R.G. Wilks,[1] M. Wimmer,[1] M. Lozach,[3] R. Félix,[1] S. Ueda,[3] H. Yoshikawa,[4] K. Lips,[1] B. Rech,[1] M. Sumiya,[3] K. Kobayashi,[3] M. Gorgoi,[1] J. Hüpkes,[2] and M. Bär[1,5]

[1]*Helmholtz-Zentrum Berlin für Materialien und Energie GmbH, Berlin, Germany*
[2]*Institut für Energie- und Klimaforschung, Forschungszentrum Jülich, Jülich, Germany*
[3]*National Institute for Materials Science (NIMS), Tsukuba, Japan*
[4]*NIMS Beamline Station, SPring-8, Hyogo, Japan*
[5]*Institut für Physik und Chemie, Brandenburgische Technische Universität Cottbus, Cottbus, Germany*

***Abstract*— The chemical and electronic properties of a-Si:C:H(B)/ZnO:Al and μc-Si:C:H(B)/ZnO:Al thin-film solar cell structures are studied by hard x-ray photoelectron spectroscopy (HAXPES). Using a combination of different x-ray excitation energies and deliberate sample design, we were able to select the probed volume, i.e. the silicon capping layer only or the silicon *and* zinc oxide layer (including the buried interface). For the a-Si:C:H(B) material, we find a higher deposition rate and a smaller value for the modified Auger parameter than for μc-Si:C:H(B). In addition, we find indications of a pronounced band bending limited to the very surface of the a-Si:C:H(B) and the μc-Si:C:H(B) layers, which is more distinct in the latter case.**

***Index Terms*—Si thin-film solar cell, HAXPES, surface and interface analysis**

I. Introduction

The interface between p-type (boron-doped) hydrogenated amorphous [a-Si:H(B)] or microcrystalline silicon [μc-Si:H(B)] and doped zinc oxide (ZnO) is found at the front contact junction of p-i-n thin-film a-Si based solar cells. These devices result in the highest efficiencies for thin-film a-Si cells to date 1. In some cases improvements in cell efficiency are observed when a p-type hydrogenated microcrystalline silicon [e.g., μc-Si:H(B)] buffer layer is introduced at this interface 23, which may be indicative of a suboptimal electronic structure at the interface between a-Si:H(B) and ZnO.

Manuscript received May 21, 2012. This work was supported in part by the Helmholtz-Association (VH-NG-423) and the German Federal Ministry of the Environment (BMU, contract numbers 0327693 and 0325299).
Corresponding authors:
D.G.: Phone: +49-(0)30-8062-42314; fax: +49-(0)30-8062-43173; e-mail: dominic.gerlach@helmholtz-berlin.de.
M.B.: Phone: +49-(0)30-8062-43824; fax: +49-(0)30-8062-43173; e-mail: marcus.baer@helmholtz-berlin.de.

Often carbon is added to the p-type Si top layer to increase its band gap, enhancing its transmission and creating a p-type "window layer" 4. Hence, we studied a-Si:C:H(B)/ZnO:Al and μc-Si:C:H(B)/ZnO:Al thin-film solar cell structures by using synchrotron-based hard x-ray photoelectron spectroscopy (HAXPES). Varying the excitation energy and the silicon capping-layer thicknesses allows for a "depth-resolved" comparative characterization, which might help to uncover the origin of the varying device performance.

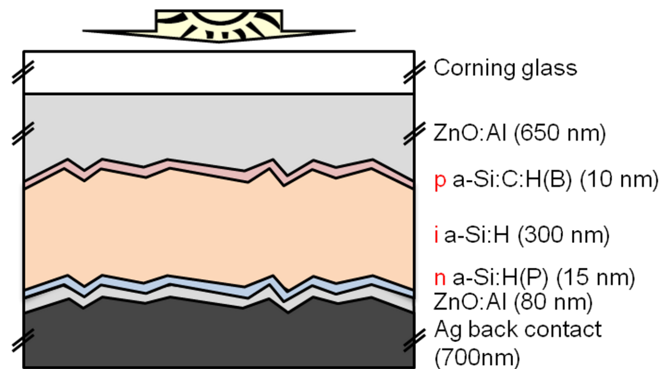

Fig. 1. Schematic of the glass/ZnO:Al/p-i-n a-Si/ZnO:Al/Ag thin-film solar cell. Simlar to 5.

II. Experimental

Using plasma-enhanced chemical vapor deposition (PECVD), boron-doped hydrogenated amorphous [a-Si:C:H(B)] and microcrystalline [μc-Si:C:H(B)] carbon-containing silicon thin layers were deposited using a mixture of SiH_4, $B(CH_3)_3$, H_2 and CO_2 [only for a-Si:C:H(B)] precursor gases. Note that we use the term "Si:C" because the material is an off-stoichiometric, very silicon-rich Si_XC_{1-X} alloy. As a

substrate a 650 nm thick aluminum-doped zinc oxide (ZnO:Al) film previously magnetron-sputtered onto a Corning Eagle glass was used 6. Different silicon layer thicknesses were produced by varying the PECVD process time between 40s and 100s for a-Si:C:H(B) and 150s and 400s for μc-Si:C:H(B).

The HAXPES measurements were performed at the SPring-8 (Beamline BL15XU 7) and BESSY II (Beamline KMC-1 8, HIKE endstation 9) synchrotron light sources. The BL15XU beamline uses a helical undulator and a double-crystal monochromator to produce intense x-rays in the range of ca. 2-36 keV, while the KMC-1 beamline uses a bending magnet and a double-crystal monochromator to generate x-rays from 2-12 keV. A VG SCIENTA R4000 hemispherical analyzer is used for electron detection at both beamlines. The energy scales were calibrated using Au 4f and Au Fermi edge reference measurements.

Using excitation energies (hν) ranging from 2 keV to 6 keV, core level photoemission spectra of the different thin-film Si/ZnO samples and a bare (i.e., uncovered) ZnO:Al reference layer were measured. The probing depth, x, is largely limited by the material- and energy-specific inelastic mean free path (IMFP) of the photoelectrons; the photoemission signal, I_0, is attenuated according to the exponential function:

$$I = I_0 e^{\frac{-x}{IMFP}} \qquad (1)$$

Hence, 95% of the signal stems from a region which corresponds to 3×IMFP, which we use as a measure for the information depth (ID) in the following. Hence, the ID of the core level spectra in this experiment ranges from 12 nm (for 2 keV excitation) to 31 nm (for 6 keV excitation) in crystalline silicon 10. Because of the dominance of the IMFP on the measurement ID compared to the much longer attenuation length of the x-rays, the measurements were performed in nearly grazing incidence geometry, with the detector oriented nearly perpendicular to the sample surface, an orientation which maximizes the signal intensity of the HAXPES measurements. The manner in which variations in Si:C:H(B) capping layer thickness and excitation energy (and therefore photoelectron kinetic energy and thus IMFP and ID) can be combined to allow a depth-resolved characterization of the chemical and electronic structure of the silicon capping layer and of the buried interface can be inferred from the schematic in Figure 2. For all combinations of excitation energy and capping layer thickness, the contributions to the recorded spectra attributable to the sample surface, Si bulk, interface, and ZnO:Al substrate will differ, as indicated by the differences in the grey area in each vicinity. The shape of the grey cone is reflective of the attenuation of the photoelectron signals recorded when measuring with the indicated excitation energy (for a given core level photoemission line – very low electron kinetic energies can of course be recorded for all excitation energies, and the ID of Auger features is independent of excitation energy).

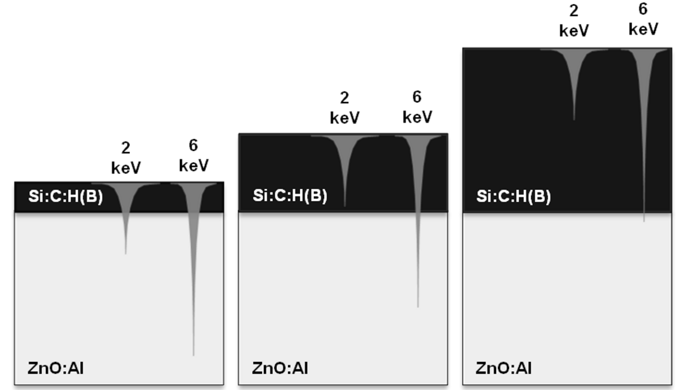

Fig. 2. Visualization of the HAXPES probing depth profiles (grey) for different excitation energies and capping layer thicknesses of the investigated Si:C:H(B)/ZnO:Al layer stacks. The vertical dimension of the probing depth cones are scaled according to the variation in electron inelastic mean free path of a particular core level excited with the given x-ray energies.

III. Results & Discussion

Survey spectra, like those of the 70s-deposited a-Si:C:H(B) sample measured at 3.2 keV and 5.9 keV excitation energy shown in Fig. 3, contain a wealth of information and were recorded for all investigated samples. In the presented spectra, we observe silicon, zinc, oxygen, and carbon photoemission lines. Most dominant for the HAXPES survey spectrum excited with 3.2 keV are the O 1s, Si 1s (not shown in this energy scale), Si 2s, and Si 2p lines. For the 5.9 keV excited measurement, Zn 2s, Zn 2p, Zn 3s, and Zn 3p increasingly contribute to the spectrum while the silicon, oxygen and carbon line intensities are reduced. These observations confirm that the 70s a-Si:C:H(B) layer completely covers the ZnO:Al bottom layer and that the excitation energy can be tuned such that only the silicon capping layer or the silicon *and* the zinc oxide (including the Si/ZnO interface) can be probed by HAXPES. From the survey spectra a C/Si ratio of 21± 5 % for both, the amorphous and microcrystalline layer, can be derived when measured with 6 keV. Note that lower excitation energy measurements showed – because of the higher surface sensitivity – a higher carbon content, possibly due to an increasing influence of C-containing surface contaminants. The composition of similarly-prepared samples have in the past been evaluated with secondary ion mass spectroscopy and shown to contain 1-5 % C in total. The increased C content observed at the surface may be due to C contamination prior to (environmental exposure) or during (adsorption of contaminants enhanced by ionization of the surface) HAXPES measurements.

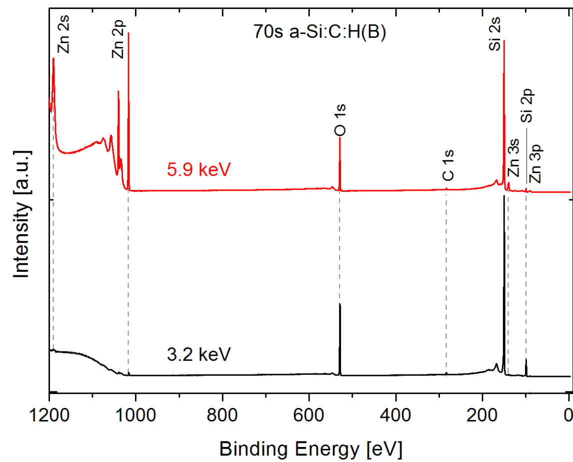

Fig. 3. HAXPES survey spectra of the 70s a-Si:C:H(B)/ZnO:Al sample measured with 3.2 keV and 5.9 keV excitation energy.

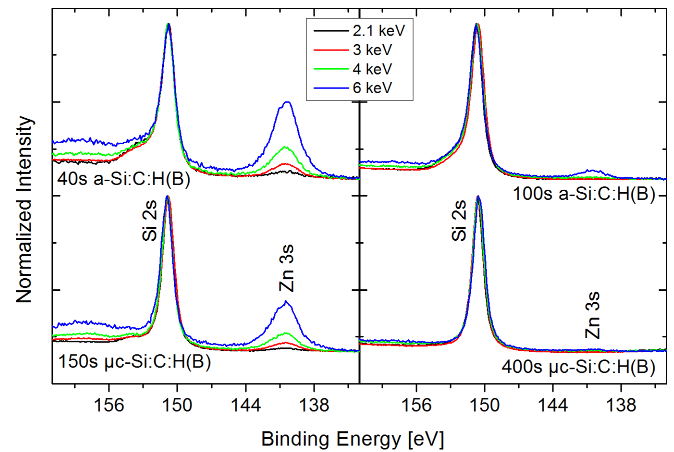

Fig. 4. Si 2s and Zn 3s HAXPES spectra of the thinnest (left) and thickest (right) samples measured at different excitation energies. The top and bottom groups of spectra correspond to the a-Si:C:H(B)/ZnO:Al and µc-Si:C:H(B)/ZnO:Al thin-film solar cell structures, respectively. The spectra are normalized to the maximum height of the Si 2s photoemission line, and the vertical offset between groups is added for clarity.

Detail spectra of the Si 2s line of the thinnest and thickest a-Si:C:H(B) (40s, 100s deposition) and µc-Si:C:H(B) (150s, 400s) layers measured at different excitation energies are shown in Fig. 4. The binding energies of the Si 2s photoemission lines range for all samples from 150.6 to 150.8 eV, in agreement with literature values (150.5 – 150.7 eV) for Si-Si bonds 11. As kinetic energy increases, the Zn 3s peak emerges from the background and increases in intensity for both pairs of samples. For the thin samples the Zn 3s is always detectable, while for the thick ones, it is only seen with the highest excitation energies confirming that, in addition to the excitation energy, also the thickness of the silicon capping layer is a valuable parameter to select the probed sample volume. No significant energy shift of the Si 2s peak (for a given sample) is observable with different excitation energies (i.e., different probing depths). Furthermore, the Si 2s lines of the amorphous silicon layers are broader than those of the microcrystalline silicon samples [e.g., 100s a-Si:C:H(B), hν = 6 keV: FWHM = (1.29 ± 0.05) eV; 400s µc-Si:C:H(B), hν = 6 keV: FWHM = (1.23 ± 0.05) eV], which can be interpreted as being indicative of the higher degree of crystallinity 15. For both types of samples (but more pronounced for the a-Si:C:H(B)/ZnO:Al sample) a shoulder at 152.5 eV and a broad feature at 158 eV (in particular for high excitation energies and the thin silicon layer sample) become more distinct. While the first can be ascribed to a more-oxidized silicon layer 1112, the latter is a normalization effect caused by the reduced intensity of the Si 2s line (which is normalized at the peak maximum) resulting in an increasing influence of the spectral background with increasing excitation energy and thus ID.

The thicknesses of the silicon capping layers were determined using the Zn 2p and Zn 3s signal attenuation. The Zn photoemission intensities of the samples were divided by those of the bare ZnO:Al reference and plotted over the excitation energy dependent inelastic mean free path 10. The respective I/I_0 ratios derived for the 270s µc-Si:C:H(B)/ZnO:Al sample are shown in Fig. 5 (left panel) as an example. Exponential fits are made, and Equation 1 is used to derive the layer thicknesses – (27.8 ± 0.4) nm in the example. The determined thicknesses of all a-Si:C:H(B) and µc-Si:C:H(B) layers are plotted in Fig. 5 (right panel) versus deposition time and listed (together with the respective deposition times) in TABLE 1. Linear fits of the data in Fig. 5 (right panel) give estimates for the deposition rates: 0.3 nm/s for a-Si:C:H(B) and 0.1 nm/s for µc-Si:C:H(B). Discrepancies between the thickness values based on our HAXPES measurements and the available thicknesses determined by spectral ellipsometry measurements (also in TABLE 1) may reflect thickness variations across the deposition area (different sample spots were measured with the two techniques). Note that two separate 40s a-Si:C:H(B) samples, deposited in two separate runs, are included in the analysis and show different thicknesses, which may be due to slightly differing deposition parameters or due to samples being taken from different spots relative to the deposition center.

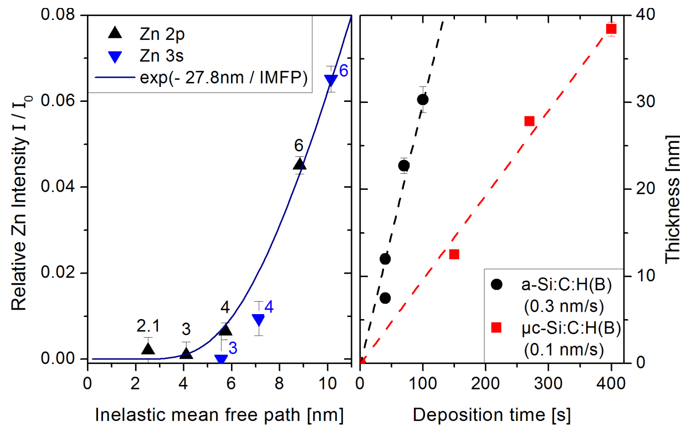

Fig. 5. Left: Relative Zn 2p and Zn 3s line intensities plotted over the inelastic mean free path 10 for the 270s μc-Si:C:H(B) sample. The exponential fit used to derive the layer thickness (see Equation 1) is shown as a dark blue solid line. The excitation energies (in keV) are indicated by the numbers next to the data points. Right: The resulting thicknesses of the a-Si:C:H(B) and μc-Si:C:H(B) capping layers are plotted over the deposition time. Dashed lines represent linear fits with the slopes given in the legend.

TABLE I

LIST OF THE INVESTIGATED SAMPLES TOGETHER WITH DEPOSITION TIME AND DETERMINED LAYER THICKNESSES.

Type	Deposition Time [s]	Thickness determined by HAXPES [nm]	Thickness determined by ellipsometry [nm]
a-Si:C:H(B)	40	7.5 ± 0.3	9.2 ± 0.5
a-Si:C:H(B)	40	12.0 ± 0.6	---
a-Si:C:H(B)	70	22.7 ± 0.9	16.9 ± 0.8
a-Si:C:H(B)	100	30.3 ± 1.5	---
μc-Si:C:H(B)	150	12.5 ± 0.3	---
μc-Si:C:H(B)	270	27.8 ± 0.4	---
μc-Si:C:H(B)	400	38.4 ± 0.8	---

In Fig. 6 the Si $KL_{2,3}L_{2,3}$ Auger and Si 1s photoelectron spectra (hν = 3 keV) of the thickest (30.3 nm) a-Si:C:H(B) sample are compared to corresponding spectra of the thickest (38.4 nm) μc-Si:C:H(B) sample. The Auger spectra are dominated by the Si $KL_{2,3}L_{2,3}$ ($^1D_2$) transition at (1616.11 ± 0.05) eV kinetic energy for a-Si:C:H(B) [(1616.22 ± 0.05) eV for μc-Si:(B)], which can be assigned to Si-Si bonds 11. The feature at approx. 1609 eV can be attributed to the accompanying $^3P_2$ Auger transition 13.

The Si 1s photoelectron spectra are dominated by the peak at a binding energy of (1839.43 ± 0.05) eV for a-Si:C:H(B) [(1839.44 ± 0.05) eV for μc-Si:(B)], which is also characteristic of Si-Si bonds 11. The broad, high-energy shoulder between 1842 and 1844 eV (more pronounced for the amorphous sample) is attributable to $Si\text{-}O_x$ bonds 11, in agreement with the interpretation of the Si 2s spectra above. The energetic distance between $Si\text{-}O_x$ and Si-Si contribution excludes SiO_2 and rather suggests the presence of a silicon suboxide (SiO_x, with x<2) 11, 12.

Furthermore, the Si 1s photoemission line [a-Si:C:H(B), hν = 6 keV: FWHM = (1.01 ± 0.05) eV; μc-Si:C:H(B), hν = 6 keV: FWHM = (0.91 ± 0.05) eV] as well as the $KL_{2,3}L_{2,3}$ Auger feature are narrower for the μc-Si:C:H(B) than for the a-Si:C:H(B) layer, again indicating a higher degree of crystallinity.

In order to evaluate the chemical information of the photoemission and Auger spectra independent of potential band bending and/or sample charging the modified silicon Auger parameter, α^*, was calculated using the kinetic energy (E_{kin}) of the Si $KL_{2,3}L_{2,3}$ ($^1D_2$) Auger and the binding energy (E_B) of the Si 1s photoemission lines, as follows:

$$\alpha^*(Si) = E_{kin}^{Si\ KL_{2,3}L_{2,3}} + E_B^{Si\ 1s} \qquad (2)$$

For the data presented in Fig. 5, the Auger parameters are (3455.53 ± 0.07) eV and (3455.66 ± 0.07) eV for the a-Si:C:H(B) and μc-Si:C:H(B) films, respecitvely. This small (but significant) α^* (Si) difference suggests the modified Auger parameter as a sensitive measure for the chemical and “structural” environment of silicon. The derived α^* (Si) values are in good agreement with the reported modified Auger parameter of silicon (3455.5 eV) 14. Note the significant difference from the modified Auger parameters for Si:C (3453.7 eV) and SiO_2 (3451.5 eV) 14.

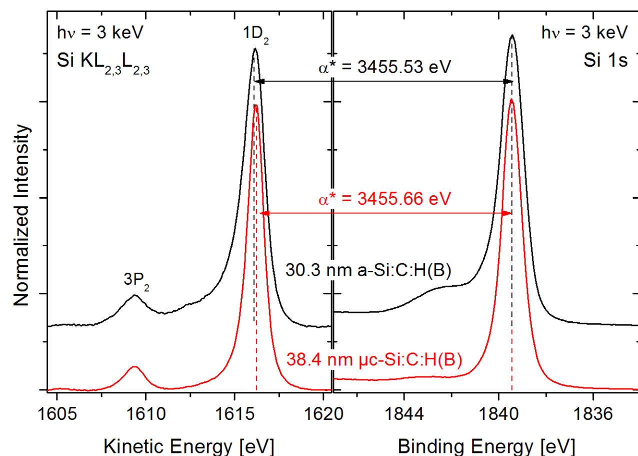

Fig. 6. Si $KL_{2,3}L_{2,3}$ Auger electron (left) and Si 1s core level (right) spectra for the thickest a-Si:C:H(B) (30.3 nm, black) and μc-Si:C:H(B) (38.4 nm, red) samples recorded using 3 keV excitation energy. The calculated modified Auger parameters (± 0.07 eV), α^*, are also shown.

Si 1s photoemission spectra measured for the thickest a-Si:C:H(B) (left panel) and μc-Si:C:H(B) (right panel) samples using different excitation energies are shown in Fig. 7. The intensity of the peak at approximately 1843 eV – ascribed to SiO_x (with x<2, see discussion above & 11, 12 – decreases with increasing excitation energy, indicating that the silicon (sub)oxide is mainly present at the sample surface. However, we have previously reported that also at the Si/ZnO interface of solid-phase crystallized polycrystalline silicon on ZnO:Al a silicon oxidation occurs 1516; thus interface oxidation can also not be excluded in this case. The more pronounced silicon oxidation of the a-Si:C:H(B) thin layers compared to that observed for the μc-Si:C:H(B) samples may indicate that amorphous silicon is more susceptible to oxidation 1718.

However, different sample handling (and thus different air exposure times) may also explain this disparity.

Furthermore, the Si 1s spectra of the a-Si:C:H(B)/ZnO:Al and µc-Si:C:H(B)/ZnO:Al samples shift (0.29 ± 0.05) eV and (0.64 ± 0.05) eV, respectively, to lower binding energies as the excitation energy increases from 2.1 keV to 6 keV. The fact that no similar shift occurs in the Si 2s lines (Fig. 4) – for which effectively constant binding energies are observed – at first sight suggests that this shift cannot be explained in a classical band bending picture, because the same shifts would be expected for all photoemission lines in that case. However, the signals in question (i.e., the Si 1s and Si 2s lines) have greatly different kinetic energies, and therefore significantly different information depths [$ID_{Si\ 1s}$ (2.1 keV) = 2.7 nm and $ID_{Si\ 2s}$ (2.1 keV) = 12.2 nm for Si 1s and Si 2s, respectively]. Hence, the more surface sensitive Si 1s photoemission line would be significantly more influenced by the presence of a surface band bending. As a consequence, we speculate that the observed deviation in the shifts of the Si 1s and Si 2s lines could therefore be indicative of a pronounced downward band bending limited to the very surface of the a-Si:C:H(B) and µc-Si:C:H(B) layers. A theoretical study as to whether this is a valid explanation and to what region such surface band bending is limited to is currently underway. The less pronounced Si 1s shift (and presumably smaller surface band bending) observed for the amorphous silicon layer could then be explained by a surface Fermi level pinning caused by the higher defect-concentration.

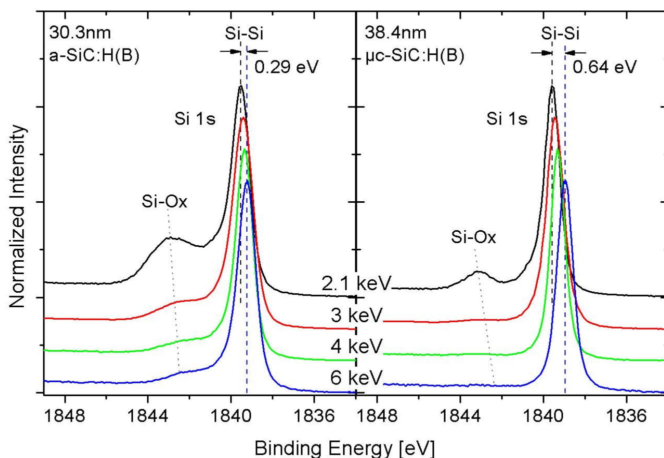

Fig. 7. Si 1s spectra of the thickest (30.3 nm) a-Si:C:H(B) (left) and (38.4 nm) µc-Si:C:H(B) (right) samples measured at various excitation energies. Excitation energy dependent shifts are indicated by the dashed vertical lines, and a vertical offset is added for clarity.

Further experimental investigations into the electronic structure (i.e., interface induced band bending and band alignment) of the Si/ZnO interface, are under way.

IV. Summary & Conclusion

Using synchrotron-based hard x-ray photoemission spectroscopy (HAXPES), the chemical and electronic structure of a-Si:C:H(B)/ZnO:Al and µc-Si:C:H(B)/ZnO:Al thin-film solar cell structures were investigated and compared. Through variation of Si layer thickness and x-ray excitation energy, we were able to deliberately control the information depth and investigate either the properties of the silicon capping layer only or that of the silicon and of the zinc oxide (including the buried interface). Using the attenuation of the Zn core level spectra the Si layer thickness of the samples (7-35 nm) and deposition rates [a-Si:C:H(B): 0.3 nm/s, µc-Si:C:H(B): 0.1 nm/s] were derived. Furthermore, we find a small but significant difference in the modified Auger parameters for a-Si:C:H(B) [(3455.53 ± 0.07) eV] and µc-Si:C:H(B) [(3455.66 ± 0.07) eV], which suggest that it could be used as a sensitive measure for the chemical *and* "structural" environment of silicon in future studies. Furthermore, the presence of excitation energy dependent binding energy shifts in surface-sensitive Si 1s and their absence in more bulk-sensitive Si 2s spectra was interpreted as an indication for a pronounced downward band bending limited to the very surface region of the a-Si:C:H(B) and µc-Si:C:H(B) thin films.

The derived "depth-resolved" information about the chemical and electronic properties of the a-Si:C:H(B) and µc-Si:C:H(B) layers and their interface to ZnO:Al may turn out to be crucial for a further rapid knowledge-based development of silicon-based thin-film solar cells.

References

[1] S. Benagli, D. Borrello, E. Vallat-Sauvain, J. Meier, U. Kroll, J. Hoetzel, J. Bailat, J. Steinhauser, M. Marmelo, G. Monteduro and L. Castens, "*High-efficiency amorphous silicon devices on lpcvd-zno tco prepared in industrial kai*^tm^*-m r&d reactor*", In Proc. 24th Eu-PVSEC, 2009, 2293-2298.

[2] K. Ellmer, A. Klein, B. Rech, *Transparent conductive zinc oxide*, Springer, 2008, p. 394

[3] J. Müller, O. Kluth, S. Wieder, H. Siekmann, G. Schöpe, W. Reetz, O. Vetterl, D. Lundszien, A. Lambertz, F. Finger, B. Rech, and H. Wagner, "Development of highly efficient thin film silicon solar cells on texture-etched zinc oxide-coated glass substrates," Solar Energy Materials and Solar Cells, vol. 66, no. 1–4, pp. 275–281, Feb. 2001.

[4] Y. Tawada, M. Kondo, H. Okamoto, and Y. Hamakawa, "Hydrogenated amorphous silicon carbide as a window material for high efficiency a-Si solar cells," *Solar Energy Materials*, vol. 6, no. 3, pp. 299–315, Mar. 1982.

[5] M. Kubon, E. Boehmer, F. Siebke, B. Rech, C. Beneking, and H. Wagner, "Solution of the ZnO/p contact problem in a-Si:H solar cells," Solar Energy Materials and Solar Cells, vol. 41–42, no. 0, pp. 485–492, Jun. 1996.

[6] M. Berginski, J. Hüpkes, M. Schulte, G. Schöpe, H. Stiebig, B. Rech, and M. Wuttig, "The effect of front ZnO:Al surface texture and optical transparency on efficient light trapping in silicon thin-film solar cells," Journal of Applied PhySi:Cs, vol. 101, no. 7, pp. 074903–074903–11, Apr. 2007.

[7] S. Ueda, Y. Katsuya, M. Tanaka, H. Yoshikawa, Y. Yamashita, S. Ishimaru, Y. Matsushita, and K. Kobayashi, "Present Status of the NIMS Contract Beamline BL15XU at SPring-8," AIP Conference Proceedings, vol. 1234, no. 1, pp. 403–406, Jun. 2010.

[8] F. Schaefers, M. Mertin, and M. Gorgoi, “KMC-1: a high resolution and high flux soft x-ray beamline at BESSY,” *Rev Sci Instrum*, vol. 78, no. 12, p. 123102, Dec. 2007.

[9] M. Gorgoi, S. Svensson, F. Schäfers, G. Öhrwall, M. Mertin, P. Bressler, O. Karis, H. Siegbahn, A. Sandell, H. Rensmo, W. Doherty, C. Jung, W. Braun, and W. Eberhardt, “The high kinetic energy photoelectron spectroscopy facility at BESSY progress and first results,” *Nuclear Instruments and Methods in PhySi:Cs Research Section A: Accelerators, Spectrometers, Detectors and Associated Equipment*, vol. 601, no. 1–2, pp. 48–53, Mar. 2009.

[10] See www.quases.com for IMFP values calculated for Si using the QUASES-IMFP-TPP2M code, which is based on S. Tanuma, C. J. Powell, and D. R. Penn, “Calculations of electron inelastic mean free paths. V. Data for 14 organic compounds over the 50–2000 eV range,” *Surface and Interface Analysis*, vol. 21, no. 3, pp. 165–176, Sep. 2004.

[11] *NIST X-ray Photoelectron Spectroscopy Database*, Version 3.5 (National Institute of Standards and Technology, Gaithersburg, MD, 2003) http://srdata.nist.gov/xps/.

[12] C. Virojanadara and L. I. Johansson, “Studies of oxidized hexagonal SiC surfaces and the SiC/SiO_2 interface using photoemission and synchrotron radiation,” *Journal of Physics: Condensed Matter*, vol. 16, no. 17, pp. S1783–S1814, May 2004.

[13] T. Eikhoff, *Photoemissionsuntersuchungen an vergrabenen Grenzschichten SiO_2/Si, SiO_2/SiC und Thiolen auf Gold mit 3,0–5,5 keV Röntgenstrahlung* , Dissertation, Universität Hamburg, 2002, p. 101

[14] G. Moretti, “Auger parameter and Wagner plot in the characterization of chemical states by X-ray photoelectron spectroscopy: a review,” *Journal of Electron Spectroscopy and Related Phenomena*, vol. 95, no. 2–3, pp. 95–144, Oct. 1998.

[15] M. Wimmer, M. Bär, D. Gerlach, R. G. Wilks, S. Scherf, C. Lupulescu, F. Ruske, R. Félix, J. Hüpkes, G. Gavrila, M. Gorgoi, K. Lips, W. Eberhardt, and B. Rech, “Hard x-ray photoelectron spectroscopy study of the buried Si/ZnO thin-film solar cell interface: Direct evidence for the formation of Si–O at the expense of Zn-O bonds,” *Applied PhySi:Cs Letters*, vol. 99, no. 15, pp. 152104–152104–3, Oct. 2011.

[16] M. Bär, M. Wimmer, R. G. Wilks, M. Roczen, D. Gerlach, F. Ruske, K. Lips, B. Rech, L. Weinhardt, M. Blum, S. Pookpanratana, S. Krause, Y. Zhang, C. Heske, W. Yang, and J. D. Denlinger, “Impact of solid-phase crystallization of amorphous silicon on the chemical structure of the buried Si/ZnO thin film solar cell interface,” *Applied PhySi:Cs Letters*, vol. 97, no. 7, pp. 072105–072105–3, Aug. 2010.

[17] A. Szekeres and P. Danesh, “Oxidation of amorphous and crystalline silicon,” *Journal of Non-Crystalline Solids*, vol. 187, no. 0, pp. 45–48, Jul. 1995.

[18] G.-R. Yang, Y.-P. Zhao, M. Abburi, S. Dabral, and B. Y. Tong, “Comparison of low-temperature oxidation of crystalline Si and B with a-Si:B alloy: An x-ray photoelectron spectroscopy study,” *Journal of Vacuum Science & Technology A: Vacuum, Surfaces, and Films*, vol. 15, no. 2, pp. 279–283, 1997.